

Nickel / Doped Ceria Solid Oxide Fuel Cell Anodes for Dry Reforming of Methane

Renata O. da Fonseca,^{a,b} Andressa A. A. da Silva,^{b,c} Matheus R. M. Signorelli,^{a,b}
Raimundo C. Rabelo-Neto,^b Fábio B. Noronha,^{*,b,c} Rita C. C. Simões^a and Lisiane V. Mattos^a

^aUniversidade Federal Fluminense, Departamento de Pós Graduação de Engenharia Química,
Rua Passo da Pátria, 156, 24210-240 Niterói-RJ, Brazil

^bInstituto Nacional de Tecnologia, Divisão de Catálise e Processos Químicos,
Av. Venezuela, 82, 20081-312 Rio de Janeiro-RJ, Brazil

^cInstituto Militar de Engenharia, Departamento de Pós Graduação de Química,
Praça General Tibúrcio, 80 - Urca, 22290-270 Rio de Janeiro-RJ, Brazil

Neste trabalho, foi estudado o desempenho catalítico de materiais a base de Ni, suportado em cério dopado com Zr, Pr e Nb para serem usados como anodos em células a combustível de óxido sólido (SOFC) alimentadas com combustíveis contendo metano e CO₂. Os anodos foram preparados pelo método hidrotérmico, usando um teor de Ni (14% em volume) menor do que o utilizado em anodos convencionais (30% em volume). Os materiais obtidos foram caracterizados através de análises de difração de raios X, redução à temperatura programada, espectroscopia Raman e termogravimetria. Os resultados mostraram que o material contendo Zr apresentou o menor tamanho de cristalito de níquel metálico, o que levou a um maior valor de atividade inicial na reação de reforma seca do metano a 1073 K. Entretanto, o catalisador Ni/CePr apresentou a menor quantidade de carbono formada. Isto foi atribuído à maior mobilidade de oxigênio do suporte CePr, o que promove o mecanismo de remoção do carbono.

In this work, the catalytic performance of Ni supported on ceria doped with Zr, Pr and Nb used as anodes for solid oxide fuel cell (SOFC) operating directly on fuels containing methane and CO₂ was studied. The anodes were prepared by a hydrothermal method using a Ni content (14 vol%) lower than that of a conventional SOFC anodes (30 vol%). The materials obtained were characterized by X-ray diffraction, temperature-programmed reduction, Raman spectroscopy and thermogravimetric analyses. The results showed that the sample containing Zr exhibited the lowest Ni crystallite size, which led to a high initial activity on dry reforming of methane at 1073 K. However, the Ni/CePr catalyst showed the lowest carbon formation. This was attributed to the higher oxygen mobility of CePr support that promotes the carbon removal mechanism.

Keywords: nickel/doped ceria, SOFC anodes, CO₂ reforming of methane

Introduction

The solid oxide fuel cells (SOFC) technology has been considered as an attractive energy conversion system. It has several advantages such as high efficiency, relatively low sensitivity to impurities, and possibility for operation with an internal reformer.^{1,2} In the case of the direct internal reforming solid oxide fuel cell (DIR-SOFC), the complexity and costs of the fuel cell system are reduced, since the available fuels (hydrocarbons or alcohols) can be fed straight to the anode side of SOFC and reformed to

H₂ without the use of an external reformer. In addition, the conversion of these fuels at the anode side can be promoted due to the H₂ consumption by the electrochemical reaction, leading to high conversions and high efficiency.³⁻⁵

Associated gas or biogas fueled SOFC system is a potential technology for electric power generation, since it can contribute to reduce CO₂ emissions. The associated gas produced in the world's largest deepwater field in Brazil contains a significant amount of carbon dioxide that has to be removed before its use. In the case of biogas or landfill gas (LFG), this gaseous mixture containing, mainly methane and carbon dioxide, is produced by anaerobic digestion or fermentation of organic matter

*e-mail: fabio.bellot@int.gov.br

such as sewage sludge, municipal solid waste (MSW), etc. Therefore, the emission of biogas to the atmosphere may contribute significantly to the greenhouse gas effect. Biogas fuelled SOFC can produce electricity with high efficiency (30-40%) even in small size power generations (< 20 kW).⁶ When associated gas or biogas is fed straight to SOFC, H₂ and CO are produced by the CO₂ reforming of methane, the so called dry reforming of methane (DRM).

The Ni/YSZ cermets are typically used as anode for SOFC systems.⁷⁻⁹ Ni provides electronic conductivity, while YSZ provides the ionic conductivity and thermal stability. However, in order to exceed the percolation threshold for electronic conductivity, a high Ni content (above 30 vol.%) is necessary. Since Ni is very active to reforming as well as cracking reactions, such a high volume fraction favors carbon formation when hydrocarbons such as methane are used directly as a fuel in SOFC. The carbon deposits on metal sites of anodes, resulting in the rapid degradation of the cell performance.^{7,8,10} It is well known that catalyst deactivation due to carbon deposition is one of the main issues of the dry reforming of methane.^{11,12} Therefore, the development of anodes for SOFC running on associated gas or biogas that exhibit high catalytic activity, high stability and adequate ionic and electronic conductivity at working conditions is still a challenge. Some strategies have been proposed for suppressing carbon deposition over SOFC anodes such as: (i) the addition of an oxidant to the feed; (ii) the decrease in Ni content and; (iii) the use of redox supports.

The use of an excess of carbon dioxide in the DRM reaction could avoid carbon deposition on the anodes.¹³ However, the use of high CO₂/CH₄ ratios decreases the electrical efficiency of the SOFC by the dilution of fuel, the yield of hydrogen and the system efficiency.¹³

Decreasing the Ni content of the anode aims at controlling the ensemble size, while keeping the appropriate electronic conductivity. The nickel particle size significantly influences the nucleation rate of carbon.¹⁴ Therefore, controlling the number of atoms in an ensemble will most likely suppress the coke formation rate. In this sense, the anode preparation method may play a critical role in determining anode stability during DRM. Some authors^{15,16} reported the use of SOFC anodes with low Ni content (ca. 10-18 wt.%) prepared by alternative methods. Jasisnky *et al.*¹⁵ showed that the conductivity under H₂ of anodes with 14 vol.% of Ni prepared by a net shape procedure was similar to the conductivity of the cermet with 35 vol.% of Ni synthesized by a conventional technique. On the other hand, Moddaferi *et al.*¹⁶ reported that Ni based anodes with low metal content (5 wt.% Ni and 5 wt.% Ru) prepared by the hydrothermal method did not exhibit carbon

formation during oxidative steam reforming (OSR) of propane under SOFC operation conditions.

Another possibility is the use of redox supports such as ceria and ceria-mixed oxides instead of YSZ in order to improve catalyst stability. These supports play an important role on the mechanism of carbon removal during DRM.¹⁷⁻¹⁹ The support participates in the dissociative adsorption of CO₂ near the metal particles, transferring oxygen to the surface of the metallic particle containing carbon deposits. Therefore, the use of supports that exhibit a high oxygen exchange capacity, such as ceria and ceria-mixed oxides, promotes the mechanism of carbon removal. Some authors^{20,21} showed that adding dopants, such as Zr, to ceria structure promotes the reduction of the bulk ceria, which was attributed to an improvement of the oxygen mobility. In addition, ceria exhibits a mixed ionic and electronic conductivity due to the reduction of Ce⁴⁺ to Ce³⁺, which improves the electrocatalytic activity of the anode. Moreover, higher ionic conductivities were obtained when ceria was doped with trivalent cations, such as Gd, Sm and Y²⁺ or Pr.²²⁻²⁵ It was also reported that doping ceria with elements of valence higher than 4+, such as Nb⁵⁺, leads to an increase of electronic conductivity.²⁶

However, only few studies reported the use of nickel/doped ceria anodes of SOFC running on methane and CO₂.^{27,28} Bornura *et al.*²⁷ detected the carbon formation on NiCu/GdCe catalysts during dry reforming of biogas at a reaction temperature ranging from 923 to 1073 K. The catalytic behavior of Ni supported on ceria-based anodes doped with Zr, Gd or Pr for methane reforming was evaluated by Gaudillèrea *et al.*²⁸ The effect of addition of water and CO₂ to a reactant mixture containing CH₄ and O₂ was studied. However, the catalytic tests were performed at very low temperatures (673-873 K) that are not typical of SOFC operating conditions. In addition, they observed that, in the presence of CO₂, most of Ni/ceria catalysts are not active.

Therefore, the aim of this work is to study the catalytic performance of Ni supported on ceria doped with Zr, Pr and Nb as anodes for SOFC operating directly on methane and CO₂. The anodes were prepared by a hydrothermal method using a Ni content (14 vol%) lower than that of a conventional SOFC anodes (30 vol%). The materials obtained were characterized by X-ray diffraction (XRD), temperature-programmed reduction (TPR) and Raman spectroscopy. Thermogravimetric analyses (TG) were carried out to measure and characterize the carbonaceous deposits formed during the reaction. The catalytic performance of the samples for DRM was evaluated, using a conventional fixed-bed reactor at the reaction temperature typical of a SOFC (1073 K).

Experimental

Catalyst preparation

The supports were synthesized by a hydrothermal method previously described elsewhere.^{16,29} An aqueous solution of precursors salts (cerium (IV) ammonium nitrate, zirconium and praseodymium nitrate, or ammonium niobium oxalate) was prepared with a Me/Ce molar ratio of 1/9 (Me = Zr, Pr or Nb). Cerium and zirconium, praseodymium or niobium hydroxides were then co-precipitated by the addition of an excess of ammonium hydroxide. The precipitate was transferred to an autoclave and heated to 453 K for 4 h. Then, the precipitate was washed with distilled water and calcined at 573 K (CeZr-573, CePr-573, CeNb-573) for 2 h in a muffle furnace. Ni (14 vol.%) was added to CeZr-573, CePr-573 and CeNi-573 supports by wet impregnation using an aqueous solution of Ni(NO₃)₂·6H₂O. After impregnation, the samples were dried at 393 K and calcined under air (50 mL min⁻¹) at 1073 K according to the following temperature program: (i) from room temperature to 673 K at 0.5 K min⁻¹; (ii) from 673 to 973 K at 1.7 K min⁻¹ and (iii) from 973 to 1073 K at 10 K min⁻¹, remaining at the final temperature for 5 h. Then, three catalysts were obtained: Ni/CeZr, Ni/CePr and Ni/CeNb. For comparison with the catalysts, the precipitates obtained after hydrothermal treatment were also calcined at 1073 K (CeZr-1073, CePr-1073, CeNb-1073).

BET surface area

The BET surface areas of the samples were measured using a Micromeritics ASAP 2020 analyzer by nitrogen adsorption at the boiling temperature of liquid nitrogen.

X-ray diffraction (XRD)

The X-ray powder diffraction pattern of the calcined and reduced/passivated samples were obtained with CuK_α radiation (λ = 1.5406 Å) using a RIGAKU diffractometer. Data were collected over the 2θ range of 25 to 75° using a scan rate of 0.04 degree step⁻¹ and a scan time of 1 s step⁻¹. The Scherrer equation was used to estimate the crystallite mean diameters of CeO₂, NiO, and Ni. For the measurements of the crystallite mean diameter of Ni, the calcined samples were also reduced under pure hydrogen (30 mL min⁻¹) at 1023 K for 1 h, purged under N₂ at the same temperature for 30 min and cooled to 298 K. Then, the reactor was maintained at 203 K by immersing it in a mixture of isopropyl alcohol and liquid nitrogen for 1 h, and the catalyst was passivated with a 5% O₂/He mixture.

Raman spectroscopy

The Raman spectra were recorded at room temperature using a Horiba LabRam HR-UV800/Jobin-Yvon spectrometer, equipped with He-Ne laser (λ = 632 nm) of intensity 10 mW, a CCD detector (203 K), Olympus BX41 microscope, objective lens of 100× and spot 0.96 nm.

Temperature-programmed reduction (TPR)

TPR measurements were carried out in a homemade apparatus. The catalyst was pretreated at 673 K for 1 h under air flow prior to the TPR experiment in order to remove traces of water. The reducing mixture (2% H₂/N₂) was passed through the sample (80 mg) at a flow rate of 30 mL min⁻¹ and the temperature was increased to 1273 K at a heating rate of 10 K min⁻¹.

Thermogravimetric analysis (TG)

Thermogravimetric analysis of the used catalysts was carried out in a TA Instruments equipment (SDT Q600) in order to determine the amount of carbon formed over the catalyst. Approximately 10 mg of spent catalyst was heated under air flow from room temperature to 1273 K at a heating rate of 20 K min⁻¹ and the weight change was measured.

Reaction conditions

CO₂ reforming of methane was performed in a quartz reactor at 1073 K and atmospheric pressure. In order to avoid hot spot formation or temperature gradients, catalyst samples (25 mg) were diluted with SiC (25 mg). Prior to the reaction, the catalyst was reduced under H₂ at 1023 K for 1 h and then heated to 1073 K under N₂. A reactant mixture with CH₄:CO₂ ratio of 1 and a flow rate of 100 mL min⁻¹ was used. The exit gases were analyzed using a gas chromatograph (Agilent 6890) equipped with a thermal conductivity detector and a Carboxen 1010 column (Supelco). The methane conversion was determined as follows:

$$X_{\text{methane}} = ((n_{\text{methane}})_{\text{feed}} - (n_{\text{methane}})_{\text{exit}}) / (n_{\text{methane}})_{\text{feed}} \times 100 \quad (1)$$

$$X_{\text{CO}_2} = ((n_{\text{CO}_2})_{\text{feed}} - (n_{\text{CO}_2})_{\text{exit}}) / (n_{\text{CO}_2})_{\text{feed}} \times 100 \quad (2)$$

Results and Discussion

Catalyst characterization

The supports calcined at 1073 K exhibited low surface areas (CeZr: 39 m² g⁻¹; CePr: 18 m² g⁻¹ e CeNb: 22 m² g⁻¹). However, these values are higher than that obtained by

Augusto *et al.*²⁹ for gadolinium-doped ceria support (ca. 8 m² g⁻¹) prepared by the same procedure used in this work. Regarding the nature of dopant, CeZr sample exhibited the highest surface area. Some authors reported that the increase in ceria surface area by the addition of zirconia is due to the higher thermal stability of CeO₂, avoiding the sintering process.^{20,21,30}

The XRD patterns of supports calcined at 1073 K are shown in Figure 1.

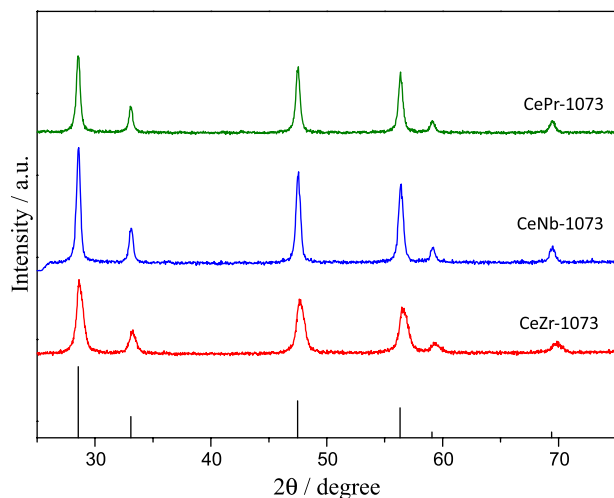


Figure 1. XRD patterns of supports calcined at 1073 K. The vertical lines corresponding to cerium oxide with cubic structure (ICSD 72155).

The diffractograms of CeZr, CePr and CeNb exhibited the diffraction lines corresponding to CeO₂. However, these lines were slightly shifted to higher 2θ positions, when the diffractograms of these samples were compared to the diffractogram of CeO₂ with cubic structure (ICSD 72155). For CeZr and CePr, these shifts indicate the formation of Ce_{0.9}Zr_{0.1}O_{1.95} (ICSD 152478) and Ce_{0.9}Pr_{0.1}O₂ (ICSD 182184) solid solutions. In the case of CeNb sample, the niobium content used (5.2 wt.%) is higher than the solubility limit of Nb in CeO₂ (1.4 wt.%), which can lead to the formation of secondary phases, such as Nb₂O₅ and CeNbO₄.²⁶ Nevertheless, the lines corresponding to Nb₂O₅ and CeNbO₄ were not detected in this work. This could be attributed to the high dispersion of these phases.

For the catalysts calcined at 1073 K, in addition to the lines related to ceria and ceria solid solutions, the XRD patterns (Figure 2) also revealed the lines characteristic of NiO phase. However, Ni/CeNb sample showed less intense lines of NiO than Ni/CeZr and Ni/CePr. This indicates that a fraction of Ni would be present as another phase such as nickel niobate. This phase was not detected in the diffractogram that is likely due to its low loading or high dispersion. Further evidences of the presence of this phase will be provided by the TPR experiments.

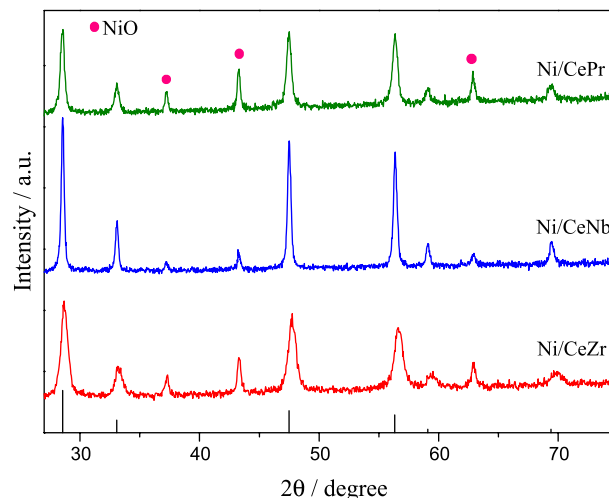


Figure 2. XRD patterns of catalysts calcined at 1073 K. The vertical lines corresponding to cerium oxide with cubic structure (ICSD 72155).

Table 1 lists the crystallite sizes calculated using the Scherrer equation for supports and catalysts, after calcination at 1073 K. For the supports, the ceria crystallite size of CeZr is smaller than that obtained for CePr and CeNb, which agrees with the values of BET surface area. These results confirm that, in the presence of Zr, the sintering process of ceria was less pronounced. In the case of catalysts, the sample containing Zr also exhibited the smallest ceria crystallite size. Moreover, adding Ni to CeZr support did not significantly affect the ceria crystallite size. On the other hand, the addition of Ni to CePr and CeNb supports led to a slight increase of ceria crystallite sizes. Ni/CeNb showed the largest NiO crystallite size (30 nm). Augusto *et al.*²⁹ obtained the same NiO crystallite size for nickel/Gd-doped ceria calcined at 1073 K.

Table 1. Crystallite sizes of CeO₂, NiO and metallic Ni phases calculated by Scherrer equation

Sample	Calcined		Reduced and passivated	
	CeO ₂ ^a / nm	NiO ^b / nm	CeO ₂ ^a / nm	Ni ^c / nm
CeZr-1073	13	–	–	–
CePr-1073	22	–	–	–
CeNb-1073	21	–	–	–
Ni/CeZr	12	24	13	24
Ni/CePr	26	22	25	33
Ni/CeNb	26	30	18	32

^aCalculated using the (111) ceria plane; ^bcalculated using the (200) NiO plane; ^ccalculated using the (111) metallic Ni plane.

The XRD patterns obtained for the reduced and passivated samples (Figure 3) exhibited the lines associated with ceria with cubic structure, CeZr and CePr solid solutions and metallic Ni phase (ICSD 43397).

The reduction treatment did not significantly change the ceria crystallite size for Ni/CeZr and Ni/CePr catalysts (Table 1). For Ni/CeNb, a decrease in the ceria crystallite size was observed. The Ni crystallite size of Ni/CeZr was smaller (24 nm) than that of Ni/CePr and Ni/CeNb (33 and 32 nm, respectively). Augusto *et al.*²⁹ also obtained a Ni crystallite size of 33 nm for nickel/Gd-doped ceria calcined and reduced at the same conditions used in this work.

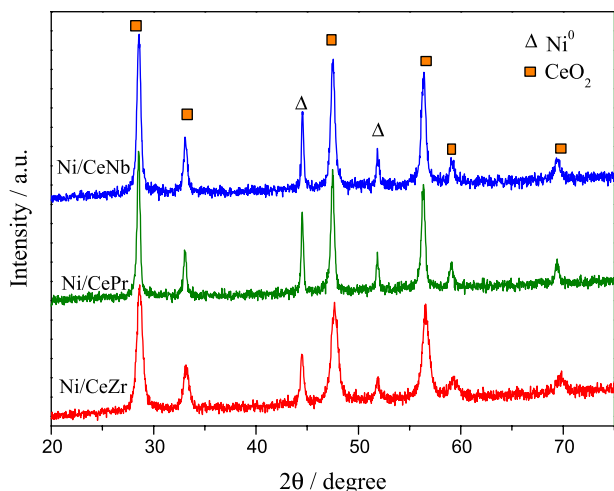


Figure 3. XRD patterns of catalysts obtained after reduction at 1023 K and passivation.

The Raman spectra of the supports are shown in Figure 4. The Raman spectrum of bulk CeO_2 was also added for comparison. CeO_2 and ceria-doped materials exhibited a band at around 465 cm^{-1} , which is associated with F_{2g} mode, due to the symmetric stretching of Ce-O vibrational unit of CeO_2 . CePr sample showed an additional broad band at 574 cm^{-1} that corresponds to defect induced mode (D band), due to oxygen vacancy.³¹ The relative intensity ratio of $I_D/I_{F_{2g}}$ is related to the degree of defect sites on

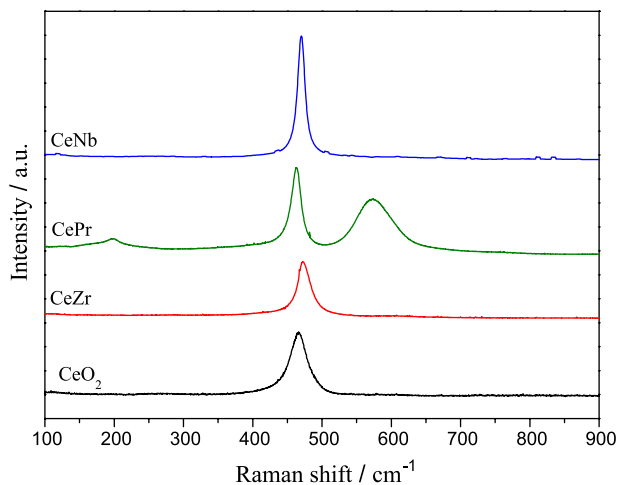


Figure 4. Raman spectra of the supports calcined at 1073 K.

CeO_2 . Then, this result indicates that the CePr sample has a higher number of oxygen vacancies.

Figure 5 shows the TPR profile of the supports calcined at 1073 K.

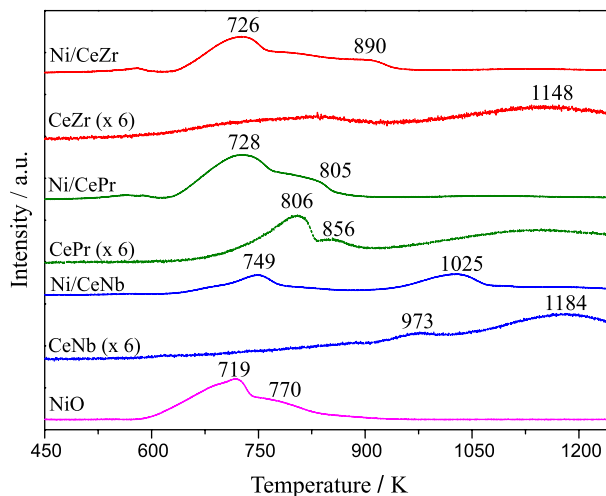


Figure 5. TPR profiles of the supports and of the catalysts calcined at 1073 K.

The TPR profile of CeZr exhibited a small H_2 consumption between 600 and 900 K and a broad peak at around 1148 K. Two peaks at 806 and 856 K and a broad H_2 uptake above 900 K were observed K in the TPR profile of CePr. For CeNb, a small H_2 consumption was also detected at 973 and 1184 K.

According to the literature,^{20,21,30} the TPR profile of CeO_2 generally exhibits a H_2 consumption at around 820 K and a large H_2 uptake at 1220 K. The H_2 consumption at low temperatures is attributed to the surface reduction of CeO_2 , whereas the H_2 uptake at high temperatures is related to the formation of Ce_2O_3 . Adding dopants, such as Zr, to ceria structure shifts the H_2 consumption to lower temperatures, which suggests that the presence of dopants promotes the reduction of ceria. This was attributed to an increase in oxygen mobility induced by the insertion of dopant into the CeO_2 lattice.

In this work, for CeZr and CePr, the H_2 consumption at low temperatures (600-900 K) was attributed to the surface reduction of CeO_2 and the H_2 uptake at higher temperatures (> 900 K) was associated with the reduction of bulk ceria. For CeNb support, the H_2 consumption at low temperatures could be also attributed to the reduction of surface ceria. However, the reduction of niobium oxide or cerium niobate at high temperature cannot be ruled out. Some authors³² observed the reduction of Nb_2O_5 around 900-1050 K.

A comparison between the TPR profiles obtained for all supports showed that CePr exhibited the highest H_2 consumption at low temperatures. In addition, a higher

reduction degree was obtained for this sample (Table 2). These results indicated that CePr showed the highest reducibility and consequently the highest oxygen mobility, which suggests that the promoting effect of ceria reduction was more significant for the sample containing Pr.

Table 2. Amount of H₂ consumed and reduction degree of the supports and NiO obtained during TPR analyses

Sample	Amount of H ₂ consumed / (mol g _{cat} ⁻¹)		Reduction degree / %
	Low temperature region (600-900 K)	High temperature region (900-1273 K)	
CeZr-1073	3.6×10^{-5}	6.0×10^{-5}	56 ^a
CePr-1073	3.8×10^{-5}	5.7×10^{-5}	57 ^a
CeNb-1073	1.2×10^{-5}	6.8×10^{-5}	44 ^a
Ni/CeZr	2.8×10^{-4}	4.5×10^{-5}	149 ^b
Ni/CePr	2.9×10^{-4}	4.9×10^{-5}	157 ^b
Ni/CeNb	1.1×10^{-4}	6.4×10^{-5}	46 ^b

^aReduction degree of CeO₂, calculated using the total amount of H₂ consumed; ^breduction degree of NiO, calculated using the amount of H₂ consumed at low temperature region.

The TPR results obtained for all catalysts were also presented in Figure 5. The TPR of a bulk NiO was also added for comparison. The TPR profile of NiO exhibited a reduction peak at 719 K and a shoulder at 770 K. The first peak was found to be much higher than the second one. In the case of Ni/CeZr and Ni/CePr catalysts, the TPR profiles were similar to the reduction profile of NiO, showing a peak at 726-728 K and a shoulder around 805-890 K. These results show the formation of large NiO particles on these catalysts, which are in agreement with the XRD results. Similar TPR profiles were obtained by Roh *et al.*³³ and Augusto *et al.*²⁹ for bulk NiO and Ni supported on ceria based oxides, indicating that there is no strong interaction between NiO and CeO₂. This was attributed to the large crystallite sizes of both support and NiO phases formed at high calcination temperatures.

The reduction degree of NiO was larger than 100% for Ni/CeZr and Ni/CePr catalysts (Table 2), which shows that the H₂ uptake at low temperature region (600-900 K) observed for these catalysts cannot be attributed only to the reduction of NiO. The H₂ consumption in this low temperature region of the TPR profiles of Ni/CeZr and Ni/CePr is likely due to the reduction of bulk NiO as well as to the reduction of CeO₂ promoted by the metallic nickel particles formed. This promoting effect is due to the hydrogen spillover from the metal particles onto the support.²¹ In the case of Ni/CeNb catalysts, in addition to the reduction of bulk NiO (749 K), it was also observed

a reduction peak at 1025 K. The reduction degree of NiO was lower than 100% (Table 2). This could be related to the presence of Ni species with lower reducibility, in addition to bulk NiO. Some authors³⁴ reported that Nb₂O₅ phase can react with nickel oxide to form a mixed niobium and nickel oxide phases, such as NiNb₂O₆ over Ni/Nb₂O₅ catalysts. The nickel niobate phase is reduced at high temperature region (1025 K). These phases were not detected in the XRD analyses, which is likely due to its low loading or high dispersion.

Reactions

Methane and CO₂ conversions as a function of time on stream (TOS) for the DRM at 1073 K over Ni/CeZr, Ni/CePr and Ni/CeNb catalysts are shown in Figure 6. The values of initial methane and CO₂ conversions obtained for Ni/CeZr (CH₄ = 74% and CO₂ = 81%) were slightly higher than that observed for Ni/CePr and Ni/CeNb (CH₄ = 66-69% and CO₂ = 75-77%). In addition, the methane and CO₂ conversions slightly decreased during 24 h TOS for all catalysts. Regarding the selectivity to H₂ and CO, all catalysts exhibited similar H₂/CO ratios (around 0.54-0.67). The values of H₂/CO ratio lower than 1.0 is likely due to the reverse of the water-gas shift reaction.

Characterization of used catalysts

TG analyses were carried out to characterize post-reaction catalysts. Figure 7 shows the TPO profiles obtained after DRM. The TPO profile of all catalysts exhibited a peak at around 899-945 K. In addition, Ni/CeNb showed a small CO₂ formation around 766 K. According to the literature,³⁵⁻³⁸ CO₂ peaks in the low temperature region (< 673 K) were attributed to oxidation of amorphous carbon overlaying the metal surface. On the other hand, the CO₂ formed at high temperatures was assigned to filamentous (773-973 K) and graphitic carbon (> 973 K). In this work, the TPO profiles after dry DRM suggest the formation of filamentous carbon for all samples.

From the TPO profiles, the amount of carbon deposited over all catalysts after DRM was calculated. Ni/CePr exhibited the lowest carbon formation (0.42 mg_{carbon} g_{cat}⁻¹ h⁻¹). The amount of carbon formed over Ni/CeNb and Ni/CeZr was 6.47 and 9.68 mg_{carbon} g_{cat}⁻¹ h⁻¹, respectively. Faria *et al.*³⁹ also detected large carbon formation over Ni/CeZrO₂/Al₂O₃ catalysts during DRM.

Some authors¹⁷⁻¹⁹ proposed a dual path mechanism for CO₂ reforming of methane. According to this mechanism, in the first step, methane dissociates on nickel surface, producing hydrogen and highly reactive carbon species

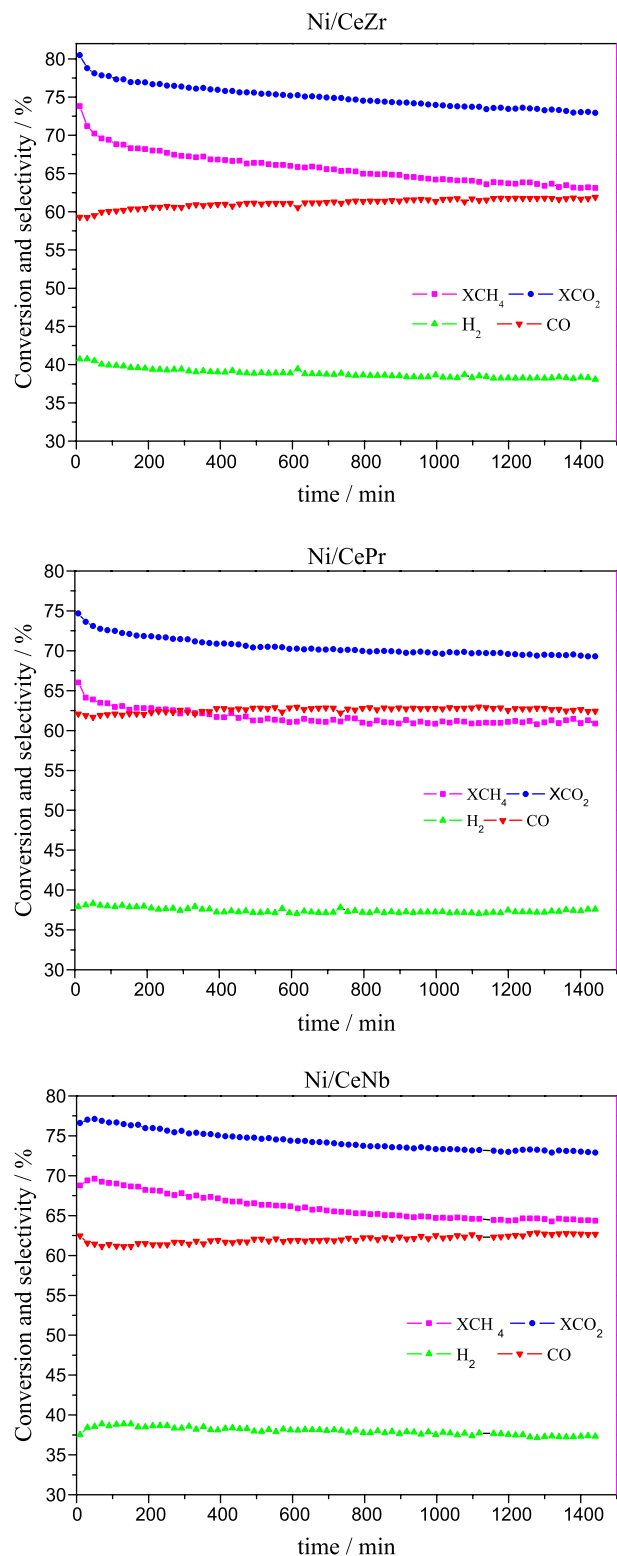


Figure 6. Methane conversion (XCH_4), CO_2 conversion (XCO_2) and products distribution versus TOS for CO_2 reforming of methane at 1073 K over Ni/CeZr, Ni/CePr and Ni/CeNb.

(C_w).⁴⁰ In the second step, this carbon reacts with oxygen from the support and the surface of the catalyst remains free of carbonaceous residues. This oxygen is formed

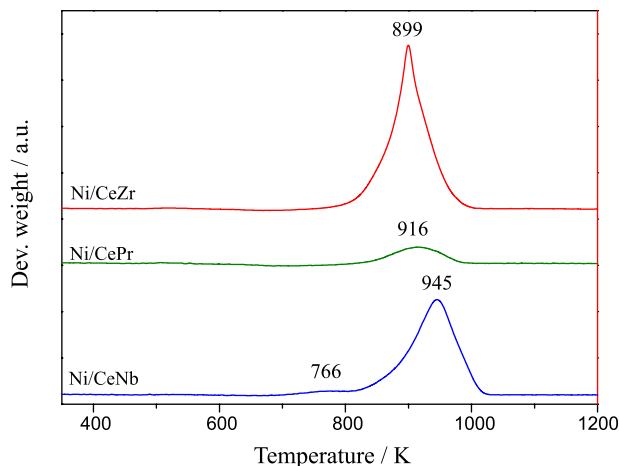


Figure 7. TPO profiles obtained during TG analyses of all catalysts after DRM at 1073 K for 24 h.

during the dissociative adsorption of CO_2 and reoxidation of the support. When the rate of methane dissociation is faster than the rate of carbon oxidation, C_α formed may undergo polymerization to less active carbon (C_β). Then, this carbon may accumulate on the surface or may dissolve into the Ni crystallite, which is the first step for the nucleation and growth of carbon filaments. Therefore, the stability of the catalyst is determined by the proper balance between the rate of methane decomposition and the rate of carbon removal. As a result, in this mechanism, the support participates in the dissociative adsorption of CO_2 near the metal particles, transferring oxygen to the coked metal and promoting the removal of carbon from the metal.^{41,42} Then, supports with a high oxygen mobility such as ceria and ceria-mixed oxides, promote the mechanism of carbon removal.

In this work, the lower carbon formation over Ni/CePr catalyst could be associated with the higher oxygen mobility of the CePr solid solution. The higher oxygen mobility of CePr support, as revealed by TPR and Raman, favors the mechanism of carbon removal, improving catalyst stability.

Conclusions

All anodes exhibited a good catalytic activity on dry reforming of methane. The values of initial methane and CO_2 conversions were slightly higher for Ni/CeZr likely due to the lower Ni crystallite size, as detected in DRX analyses. However, all samples presented a slight deactivation during the reaction. The TG analyses carried out after the reaction showed that this loss of activity was due to the formation of carbon that was lower for the sample containing Pr. This result was attributed to a higher reducibility and a higher amount of oxygen vacancies on Ni/CePr catalyst, as revealed by TPR and Raman analyses. A significant

increase in oxygen mobility was induced by the insertion of Pr into the CeO₂ lattice. The higher oxygen mobility of Ni/CePr promoted the mechanism of carbon removal, reducing the amount of carbon formed during the reaction.

Acknowledgements

The authors (R. O. da Fonseca, A. A. A. da Silva, M. R. M. Signorelli and R. C. Rabelo-Neto) acknowledge the scholarship received from CAPES, CNPq and FAPERJ.

References

- Laosiripojana, N.; Assabumrungrat, S.; *J. Power Sources* **2007**, *163*, 943.
- Suna, C.; Stimming, U.; *J. Power Sources* **2007**, *171*, 247.
- Tsiakaras, P.; Demin, A.; *J. Power Sources* **2001**, *102*, 210.
- Douvarzides, S. L.; Coutelieris, F. A.; Demin, A. K.; Tsiakaras, P. E.; *Int. J. Hydrogen Energy* **2004**, *29*, 375.
- Arpornwichanop, A.; Chalermpanchai, N.; Patcharavorachot, Y.; Assabumrungrat, S.; Tade, M.; *Int. J. Hydrogen Energy* **2009**, *34*, 7780.
- Piroonlerkgula, P.; Laosiripojanab, N.; Adesinac, A. A.; Assabumrungrata, S.; *Chem. Eng. Process.* **2009**, *48*, 672.
- Minh, N. Q.; *J. Am. Ceram. Soc.* **1993**, *76*, 563.
- Atkinson, A.; Barnett, S.; Gorte, R. J.; Irvine, J. T. S.; Mcevoy, A. J.; Mogensen, M.; Singhal, S. C.; Vohs, J. M.; *Nat. Mater.* **2004**, *3*, 17.
- Park, S.; Vohs, J. M.; Gorte, R. J.; *Nature* **2000**, *404*, 265.
- Lanzini, A.; Leone, P.; Guerra, C.; Smeacetto, F.; Brandon, N. P.; Santarelli, M.; *Chem. Eng. J.* **2013**, *220*, 254.
- Lercher, J. A.; Bitter, J. H.; Steghuis, A. G.; Van Ommen, J. A.; Seshan, K. In *Catalytic Science Series*; Janssen, F. J. J.; Van Santen, R. A., eds.; Imperial College Press: London, England, 1999.
- Bradford, M. C. J.; Vannice, M. A.; *Catal. Rev.: Sci. Eng.* **1999**, *41*, 1.
- Assabumrungrat, S.; Laosiripojana, N.; Piroonlerkgul, P.; *J. Power Sources* **2006**, *159*, 1274.
- Rostrup-Nielsen, J. R.; Sehested, J.; Norskov, J.; *Adv. Catal.* **2002**, *47*, 65.
- Jasinski, P.; Suzuki, T.; Petrovsky, V.; Andersonb, H. U.; *Electrochem. Solid-State Lett.* **2005**, *8*, 21.
- Modafferi, V.; Panzera, G.; Baglio, V.; Frusteri, F.; Antonucci, P. L.; *Appl. Catal., A* **2008**, *334*, 1.
- Stagg-Williams, S. M.; Noronha, F. B.; Fendley, G.; Resasco, D. E.; *J. Catal.* **2000**, *194*, 240.
- Ross, J. R. H.; van Keulem, A. N. J.; Hegarty, M. E. S.; Seshan, K.; *Catal. Today* **1996**, *30*, 193.
- O'Connor, A. M.; Meunier, F. C.; Ross, J. R. H.; *Stud. Surf. Sci. Catal.* **1998**, *119*, 819.
- Passos, F. B.; Oliveira, E. R.; Mattos, L. V.; Noronha, F. B.; *Catal. Today* **2005**, *101*, 23.
- Kaspar, J.; Fornasiero, P.; Graziani, M.; *Catal. Today* **1999**, *50*, 285.
- Rocha, R. A.; Muccillo, E. N. S.; *Ceramica* **2001**, *47*, 219.
- Yashiro, H.; Eguchi, Y.; Eguchi, K.; Arai, H.; *J. Appl. Electrochem.* **1998**, *18*, 527.
- Inaba, H.; Tagawa, H.; *Solid States Ionics* **1996**, *83*, 1.
- Ftikos, C.; *J. Eur. Ceram. Soc.* **1993**, *12*, 267.
- Ramirez-Cabrera, E.; Atkinson, A.; Chadwick, D.; *Catal. Today* **2002**, *36*, 193.
- Bonura, G.; Cannilla, C.; Frusteri, F.; *Appl. Catal., B* **2012**, *121*, 135.
- Gaudillère, C.; Vernoux, P.; Mirodatos, C.; Caboche, G.; Farrusseng, D.; *Catal. Today* **2010**, *157*, 263.
- Augusto, B. L.; Costa, L. O. O.; Noronha, F. B.; Colman, R. C.; Mattos, L. V.; *Int. J. Hydrogen Energy* **2012**, *37*, 12258.
- Hori, C. E.; Permana, H.; Ng Simon, K. Y.; Brenner, A.; More, K.; Rahmoeller, K. M.; Belton, D.; *Appl. Catal., B* **1998**, *16*, 105.
- Du, X.; Zhang, D.; Shi, R.; Gao, Z. J.; *J. Phys. Chem. C* **2012**, *116*, 10009.
- Wojcieszak, R.; Jasik, A.; Monteverdi, S.; Ziolk, M.; Bettahar, M. M.; *J. Mol. Catal. A: Chem.* **2006**, *256*, 225.
- Roh, H. S.; Jun, K. W.; Dong, W. S.; Park, S. E.; Joe, Y. I.; *J. Mol. Catal. A: Chem.* **2002**, *181*, 137.
- Savova, B.; Loridant, S.; Filkova, D.; Millet, J. M. M.; *Appl. Catal., A* **2010**, *390*, 148.
- Fatsikostas, A. N.; Verykios, X. E.; *J. Catal.* **2004**, *225*, 439.
- Galetti, A. E.; Gomez, M. F.; Arrua, L. A.; Abello, M. C.; *Appl. Catal., A* **2008**, *348*, 94.
- Sanchez-Sanchez, M. C.; Navarro, R. M.; Fierro, J. L. G.; *Int. J. Hydrogen Energy* **2007**, *32*, 1462.
- de Lima, S. M.; da Silva, A. M.; da Costa, L. O. O.; Assaf, J. M.; Jacobs, G.; Davis, B. H.; Mattos, L. V.; Noronha, F. B.; *Appl. Catal., A* **2010**, *377*, 181.
- Faria, E. C.; Neto, R. C. R.; Colman, R. C.; Noronha, F. B.; *Catal. Today* **2014**, *228*, 138.
- Trimm, D. L.; *Catal. Today* **1997**, *37*, 233.
- Noronha, F. B.; Fendley, E. C.; Soares, R. R.; Alvarez, W. E.; Resasco, D. E.; *Chem. Eng. J.* **2001**, *82*, 21.
- Bitter, J. H.; Hally, W.; Seshan, K.; van Ommen, J. G.; Lercher, J. A.; *Catal. Today* **1996**, *29*, 732.

Submitted on: August 5, 2014

Published online: October 21, 2014